

VGMSHield: Mitigating Misuse of Video Generative Models

A Multi-Faceted Approach through Fake Video Detection, Tracing, and Prevention

Yan Pang[†], Yang Zhang[‡], and Tianhao Wang[†]

[†]University of Virginia [‡]CISPA Helmholtz Center for Information Security
{yanpang, tianhao}@virginia.edu, zhang@cispa.de

Abstract

With the rapid advancement in video generation, people can conveniently utilize video generation models to create videos tailored to their specific desires. Nevertheless, there are also growing concerns about their potential misuse in creating and disseminating false information.

In this work, we introduce VGMSHield: a set of three straightforward but pioneering mitigations through the life-cycle of fake video generation. We start from *fake video detection* trying to understand whether there is uniqueness in generated videos and whether we can differentiate them from real videos; then, we investigate the *tracing* problem, which maps a fake video back to a model that generates it. Towards these, we propose to leverage pre-trained models that focus on *spatial-temporal dynamics* as the backbone to identify inconsistencies in videos. Through experiments on seven state-of-the-art open-source models, we demonstrate that current models still cannot perfectly handle spatial-temporal relationships, and thus, we can accomplish detection and tracing with nearly perfect accuracy.

Furthermore, anticipating future generative model improvements, we propose a *prevention* method that adds invisible perturbations to images to make the generated videos look unreal. Together with fake video detection and tracing, our multi-faceted set of solutions can effectively mitigate misuse of video generative models. Our code is available¹.

1 Introduction

With the significant success of diffusion models in the field of image generation, increasing attention is being directed towards video generation tasks. Diffusion-based video generation models have seen substantial development in the past year, with many novel model architectures being introduced. Current public state-of-the-art models, such as Stable Video Diffusion [3] and Videocrafter [10], are now capable of producing reasonable and high-resolution videos. Recently, Ope-

nAI publishes demos of Sora², capable of generating minute-long photorealistic videos.

As video diffusion models rapidly evolve, concerns regarding its misuse cannot be overlooked. Malicious individuals could utilize these models to create and disseminate fake videos online for instigation and malicious propaganda. Such actions undoubtedly pose a severe threat. Similar threats also exist in other areas of generative content [46]. Efforts have been made to tackle these threats. For example, in image generation [5, 13, 18, 19, 21, 28, 42, 49], audio synthesis [44, 56], and text generation [31, 38]. However, to date, no research has addressed the misuse of samples generated from general video generative models.

In this work, we propose VGMSHield, a set of three straightforward but pioneering mitigations through the lifecycle of fake video generation. We first delineate three roles based on the life-cycle of generated content: *Consumer*, *Modifier*, and *Creator*. Initially, there (optionally) exists original content created by *Creator*, mostly for benign purposes like sharing. The malicious *Modifier* then takes the generative model to create fake content (in our context, videos). Finally, *Consumer* reads those contents. We have a more detailed discussion in [Figure 1 in Section 2](#).

For *Consumer*, we design *fake video detection* to empower them in distinguishing fake videos. We consider three detection models that use pre-trained video recognition models to extract spatial-temporal features. These pre-trained models serve as the backbone, linked to fully connected layers for detection. Upon evaluating these detection models in four detection scenarios that mirror real-world conditions, we categorized scenarios based on the background knowledge of the model and data, as detailed in [Section 3.2.1](#). Notably, MAE-based detection model consistently outperformed the others.

Moreover, we consider the *tracing* problem that identifies which model the generated content comes from. The intuition is different models exhibit different features when generating videos. Tracing can also potentially help with the regulation

¹<https://github.com/py85252876/MMVGM.git>

²<https://openai.com/sora>. Unfortunately, it is not ready for use by the public yet.

of generative models (by identifying which models are being misused). Similar to building our detection models, tracing models are also based on pre-trained video recognition models as backbones. MAE-based models show effectiveness in tracing, can achieve 97% accuracy in *data-aware* setting. Even in the more realistic setting, it can still achieve 90% accuracy.

To investigate why our detection and tracing models are effective and the reasons behind performance differences across different backbone models, we then employ the Grad-CAM [48] technique for a detailed analysis. Grad-CAM is a widely used explainability method that helps understand why models make specific decisions on inputs. It highlights regions of the input that receive more attention during the model’s running (more details in Section 3.4.2). By applying Grad-CAM to several representative samples, we observe distinct traits of the MAE-based detection model [54]. It shows versatility in detection capabilities and heightened sensitivity to temporal distortions.

Finally, for *Creator*, we introduce *misuse prevention* to disrupt generation, thereby safeguarding the integrity of content originated by *Creator*. Following the previous work in protecting image assets [33, 50]. We also add the perturbation to the image. However, given the processing nature, there are differences between video generation models and image generators. The motion prediction term needs to be considered in our work. We designed two defense strategies within our setting, both of which demonstrated robust defensive capabilities in our experiments. Our comprehensive pipeline is evaluated on two publicly available high-quality video datasets. It encompasses seven open-source and two commercial video generation models, covering eleven distinct generation tasks.

Contributions. The contributions of our work are:

- We introduce the first defense pipeline specifically designed for samples generated by general video generation models, comprising three key components: *fake video detection*, *tracing*, and *prevention*. The *fake video detection* component comprehensively considers four real-world scenarios and is designed with four distinct variants. The *tracing* feature can trace the origin of a video based on subtle differences in the content. Meanwhile, *prevention* offers two different defense methods, both of which provide effective protection against various video generation models.
- Our work systematically evaluates the effectiveness of the proposed methods, incorporating two open-source datasets, seven open-source models, and eleven generative tasks, including text-to-video and image-to-video. Based on the observed results, we provide an analysis of how to effectively detect generated videos and safeguard sensitive images.

Roadmap. Section 2 provides preliminary knowledge and outlines the problem we aim to investigate. Section 3 delves into and analyzes our proposed fake detection method and

fake source tracing model. From the perspective of *Creator*, we introduce and evaluate defense strategies against image-to-video generation in Section 4. Section 5 summarizes related work on the detection of AI-generated content and video diffusion models. In Section 6, we discuss our study’s limitations and conclude our work.

2 Background

2.1 Denoising Diffusion Generation Models

Diffusion models [26] encompass two primary processes: the forward diffusion process, and the reverse denoising process, which progressively removes noise from an image, ultimately generating the final output.

The forward process can be conceptualized as a Markov chain. Starting with the input image x_0 , the noisy image at time t , denoted as x_t , is dependent solely on the noised output from the previous moment, x_{t-1} :

$$x_t = \sqrt{\alpha_t}x_{t-1} + \sqrt{1 - \alpha_t}\epsilon; \quad \epsilon \sim \mathcal{N}(0, 1) \quad (1)$$

where α_t is a pre-defined noise schedule. Subsequently, employing the reparameterization trick enables the direct derivation of the noised image at time t from the original image x_0 , which can be expressed as follows:

$$x_t = \sqrt{\bar{\alpha}_t}x_0 + \sqrt{1 - \bar{\alpha}_t}\epsilon_t; \quad \epsilon_t \sim \mathcal{N}(0, 1) \quad (2)$$

In the denoising process, a neural network (e.g., UNet) ϵ_θ is trained to predict ϵ_t given the input x_t and time step t , thereby achieving a reduction in noise level to obtain x_{t-1} . In the inference process, only the denoising process is needed. The diffusion process is used to get x_t during training the $\epsilon_\theta(x_t, t)$:

$$L_t(\theta) = \mathbb{E}_{x_0, \epsilon_t} \left[\|\epsilon_t - \epsilon_\theta(\sqrt{\alpha_t}x_0 + \sqrt{1 - \alpha_t}\epsilon_t, t)\|_2^2 \right] \quad (3)$$

More details about diffusion models can be found at Appendix A.

Video Generation Model using Diffusion Models. Videos are essentially sequences of images. Current video generation models predominantly adopt the architecture of diffusion models with temporal layers for video synthesis [3, 4, 10, 11, 14, 24, 25, 27, 41, 52, 60, 61, 66, 67, 72]. Video diffusion models of this kind inherit their *spatial* domain understanding from diffusion models, and integrate a *temporal* convolution layer into each UNet block, to produce videos.

In Table 1, we summarize nine generative tasks across seven models. To our knowledge, all of these are currently open-source state-of-the-art video generation models. These models accept prompts or images through an encoder (e.g., CLIP [45]) as conditional inputs to guide the generation of videos with frame number ranging from 16 to 96. The generated videos’ duration is from 2 to 4 seconds. Note that OpenAI’s Sora seems much more powerful (generating minute-long and photorealistic videos) in their demo, but it is not

Table 1: Representative open-source generative tasks, detailing for task category, video resolution, and frame rate. ‘I’ refers to Image, and ‘T’ denotes Text.

Model	Open Sourced	Input	Video Resolution	# Frames
HotShot-xl [41]	✓	T	672 × 384	16
I2VGen-xl [67]	✓	T	448 × 256	16
Lavie [61]	✓	I + T	1280 × 704	16
Seine [11]	✓	T	512 × 320	16
Seine [11]	✓	I	560 × 240	16
Show-1 [66]	✓	T	576 × 320	24
Stable Video Diffusion [3]	✓	I	1024 × 576	25
Videocrafter [10]	✓	I + T	512 × 320	28
Videocrafter [10]	✓	T	1024 × 576	28
Gen-2 ³	✗	I + T	768 × 448	96
Pika Lab ⁴	✗	I + T	1024 × 576	72

open to the public. While our evaluation does not include Sora, we believe the methodology and conclusion/insights also apply to Sora.

Note that there are also video *modification* models that take videos as input. These models can modify the object or motion depicted in the original footage [9, 30, 34, 39, 51, 64, 69–71]. For instance, video editing models are capable of transforming the content from ‘A man playing basketball’ to ‘A panda playing basketball’ throughout the video. This work focuses on generative models that take images and/or text as input.

2.2 Problem Statement

We start by modeling parties in real-world scenarios into three distinct entities: Creator, Modifier, and Consumer, following the life-cycle of information/content generation and consumption. Figure 1 provides a demonstration of the roles of these three entities. For example, photographers or journalists can be the Creator. They upload information for the Consumer. However, due to the presence of Modifier, a portion of the images they upload may be maliciously used to generate fake videos mislead Consumer (e.g., they could have topical controversy and sway public opinion).

To address the safety concerns posed by video generation models, we propose a comprehensive defense framework comprising three distinct approaches. These include *fake video detection*, *fake video source tracing*, and *misuse prevention*.

- *Fake video detection*: The detection method primarily informs Consumer about the authenticity of the videos they are viewing, discerning whether they are AI-generated.
- *Fake video source tracing*: Tracing informs Consumer about the specific AI model that produced a video, should it be AI-generated.
- *Misuse prevention*: For defense against image-to-video generative tasks, we introduce our method that adds perturbations across both spatial and temporal dimensions to safe-

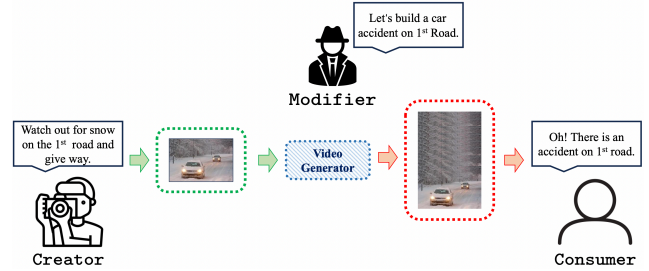


Figure 1: We assume there are three parties: Consumer, Creator, and Modifier. In a typical scenario, Creator create images, e.g., road with snow to notify people to take care, and publish them; Modifier take those content and create videos for malicious purposes, e.g., video of car accident; when Consumer see the malicious videos, they may be scared.

guard images, thereby preventing video generation models from successfully inferring videos from these input images.

Technically, detection and tracing are both classification tasks; we will describe them together.

3 Fake Video Detection and Tracing

In the realm of image generation models, it is observed that images produced by different models exhibit distinguishable variations in the frequency domain [49]. We posit this fact can transfer to video generation: *videos created by generative models will possess unique, model-specific characteristics across the spatiotemporal dimensions*. We aim to leverage these traits for video detection and source tracing. Firstly, we analyze and categorize different scenarios.

3.1 Threat Model Categorization

3.1.1 Detection

We categorize the task of detection based on the availability of two types of background knowledge: (1) where the target video comes from, and (2) from which model the target video is generated. These two types of information are not always reasonable assumptions in real-world scenarios; we consider them more for a comprehensive understanding of the technique. The four settings are summarized in Table 2.

Targeted Detection. In this scenario, detectors have knowledge of the potential models that could have generated a given video (if it is an AI-generated video). Additionally, the data source used to generate this video is also informed. This scenario is highly idealized.

D-blind. In this setting, detectors may know where the video is generated from but lack information about the data (image and/or text) distribution that is used to generate fake videos.

Table 2: Summary of different scenarios for fake video detection and tracing. ‘Data’ indicates the distribution of the data source (e.g., the fake videos are generated from images from a specific movie), and ‘Model’ indicates the generating model. ✓: Known, ✗: Unknown.

Task	Setting	Data	Model
Fake Video Detection	Targeted detection	✓	✓
	D-blind	✗	✓
	M-blind	✓	✗
	Open detection	✗	✗
Video Source Tracing	Data-aware	✓	✗
	Data-agnostic	✗	✗

For example, detectors might speculate that SVD [3] is used to generate fake videos on specific topics, because it is the current state-of-the-art open sourced model. We simulate the D-blind setting by training the detection method on one real/fake video dataset but testing it on another dataset.

M-blind. Similarly, M-blind indicates situations where the generation model is unknown, but the source of the data (distribution) is known.

Open Detection. Lastly, open detection considers the most challenging and perhaps most realistic scenario, where both the data source and the model are unknown.

3.1.2 Source Tracing

Tracing leverages the characteristics of fake videos to locate the origin of the video generation model. Thus, due to the inherent nature of this task, the generative models are, by default, set to unknown, leaving us with two scenarios. To differentiate from detection tasks, we call them *data-aware* and *data-agnostic* settings (bottom two rows in Table 2).

3.2 Methodology

We have reformulated detecting fake videos and tracing fake video generation models as a classification task. We postulate that *fake videos exhibit spatial anomalies and manifest temporal inconsistencies and anomalies*. Hence, we adopt pre-trained video recognition models with capabilities to understand spatial and temporal dynamics to serve as the backbone for our detection and source tracing models. In this paper, we use Inflated 3D ConvNet (I3D) [8], X-CLIP (X-CLIP) [36], and Video Masked Autoencoders (MAE) [54]. We defer more details of these models to Appendix B.

Denote the pre-trained video recognition model as ϵ (ϵ can be I3D, X-CLIP, or MAE), we straightforwardly connect them with trainable, fully connected layers w , and obtain the final detection model $f = w \cdot \epsilon$ (to denote $f(x) = w(\epsilon(x))$). During the training phase, we freeze ϵ and only modify w .

3.2.1 Detection

Given the base model f , the detailed constructions to handle different scenarios (listed in Table 2) differ only in how to train the model. There are only two generic principles that probably apply to all classification problems:

- *The training set should be as diverse as possible.* This applies to the open detection setting, where we curate as many real and fake videos as possible.
- *When the task is more specific, the training set should be narrowed to match the task.* This applies to the settings when the detector has knowledge about the model being used and/or distribution of the data to generate the videos. In those settings, the training set only includes videos generated from the same model and/or same distribution.

More concretely, as will be detailed later in Section 3.3, we have $G = \{G_0, \dots, G_8\}$ of 9 tasks and $D = \{D_0, D_1\}$ of 2 video datasets. For each real video in the video dataset, we generate their corresponding fake videos. Specifically, we use the images (first frame) and (if applicable) captions to query each video generation model to produce fake videos. This is to minimize the distance between real and fake videos (to minimize the detector’s reliance on other features, e.g., real videos are always about animals while fake ones are always about cars). The paradigm is shown in Figure 2.

Once the training set is constructed, we can train f for different scenarios following the abovementioned principles. To simulate the case where the data distribution is unknown, we train f on real/fake videos from one dataset D_b ($b \in \{0, 1\}$) and test on the other dataset $D_{\bar{b}}$; for the case where the model is unknown, we train f using real videos and fake videos generated from a subset of the 9 tasks $G_s \subset G$, and test on fake videos generated from the remaining models $G \setminus G_s$.

3.2.2 Source Tracing

Technically, *fake video source tracing* is very similar to *fake video detection*, as they are both classification models. However, there are some differences.

First, tracing assumes the data (video) is always fake, and f becomes a *multi-label* classification model. Second, because here the task is to guess which one of the 9 models the fake video comes from, although the model is set to unknown, the training of f always involves fake videos generated from all 9 models. This is different from the M-blind setting in detection, where the generative model used in testing is not used during training.

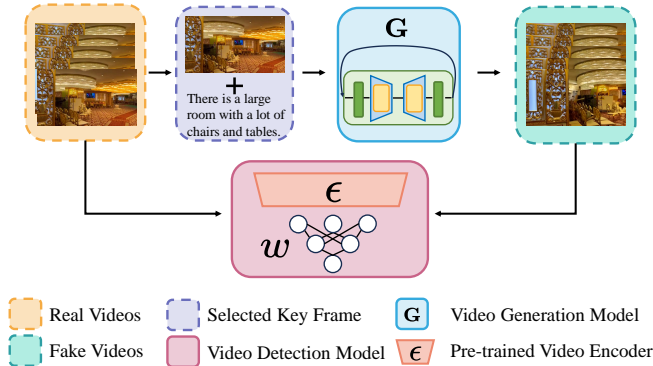


Figure 2: Experimental pipeline for fake video detection. To make sure real and fake videos follow similar distribution, we generate fake videos using the first frame of a real video (and optionally the associated caption). The classification model is composed of a video recognition model as the backbone, and a fully connected model, trained on those real/fake videos.

3.3 Evaluation

3.3.1 Experiment Setup

Datasets We consider two datasets, both are traditional video-caption datasets that have been extensively used in training and evaluation on these models [10, 52, 59, 61, 67].

- **WebVid-10M** [1]. WebVid-10M is a fundamental dataset in the field of video-text alignment and understanding. As a comprehensive collection, it comprises 10 million video clips, totaling 52,000 hours. Each clip is accompanied by descriptive text, making it a useful resource for training and evaluating machine learning models. WebVid-10M is particularly notable for its scale and diversity. It offers a broad spectrum of content that challenges and enhances algorithm capabilities in understanding the intricate relationship between visual and textual data.
- **InternVid** [62]. InternVid is a large-scale, video-centric multimodal dataset. It is designed to facilitate learning robust and transferable video-text representations, crucial for multimodal understanding and generation tasks. Including over 7 million videos with a cumulative duration of nearly 760,000 hours, the dataset offers 234 million video clips. Each clip is coupled with text descriptions, totaling approximately 4.1 billion words.

Evaluation Setting. As shown in Table 1, we have collected all the open-sourced video generation models, including I2VGen-xl [67], Videocrafter [10], Show-1 [66], Hotshot-xl [41], Stable Video Diffusion (SVD) [3], Lavie [61], Seine [11]. These models can generate videos based on conditional text [10, 41, 66, 67] or images [3, 10, 11, 67]. Specifically, I2VGen-xl and Videocrafter can input

Table 3: Experiment details.

Parameters	I3D	X-CLIP	MAE
Input frame	16	8	16
Training epoch	20	20	20
Learning rate	10^{-4}	10^{-4}	10^{-4}
Optimizer	Adam	Adam	Adam
Resolution	224×224	224×224	224×224
Warmup steps	1000	1000	1000
Detection run time (seconds)	≈ 689	≈ 10700	≈ 3700
Tracing run time (seconds)	≈ 2907	≈ 48353	≈ 16043

both images and prompts to synthesize videos. Therefore, we have nine video generation tasks, for each of which we infer 1000 videos using every dataset. We want to clarify here that there is no data overlap between each generation task. Due to the need to change code that fit our own task, we conducted our *fake video detection* and *fake video source tracing* tasks on these nine generation tasks. The two closed-source models were used to test the robustness of *misuse prevention*.

All experiments will be conducted using 4 Nvidia A100 GPUs. Our datasets are both video-caption datasets and do not supply image data. Hence, for image-to-video generation models, we will clip the first frame of the video to use as the image input that queries the model. More experiment details for our *fake video detection* and *fake video source tracing* models are shown in Table 3. The I3D⁵, X-CLIP⁶, and MAE⁷ models have been adapted from their original code repositories. Similarly, Grad-CAM⁸ has also been appropriately modified for use in our tasks to assist in analysis.

3.3.2 Detection

Targeted Detection. We conducted targeted detection for 9 video generative tasks, using 3 detection models and 2 datasets, a total of 54 tasks. The results are shown in Figure 3. Among the three detection models, differences in pre-training datasets and parameter settings constrain X-CLIP [36] to input only 8 frames for assessment. In contrast, I3D [8] and MAE [54] can accommodate 16-frame video inputs. Focusing on the video sample using the WebVid dataset [1], we observe that all three detection models achieve near-perfect detection success rates. These rates are close to 100% across 9 generative tasks under investigation. Only in certain tasks, such as X-CLIP on WebVid-Seine-T2V [11] and I3D on Webvid-I2VGen-xl-I2V [67], do the accuracy rates drop below 80%.

In experiments conducted on videos generated from the InternVid dataset [62], we noticed a significant drop in detection success rates compared to the WebVid dataset [1]. Remark-

⁵https://github.com/v-iashin/video_features

⁶<https://github.com/microsoft/VideoX>

⁷https://huggingface.co/docs/transformers/en/model_doc/videomae

⁸<https://github.com/facebookresearch/SlowFast>

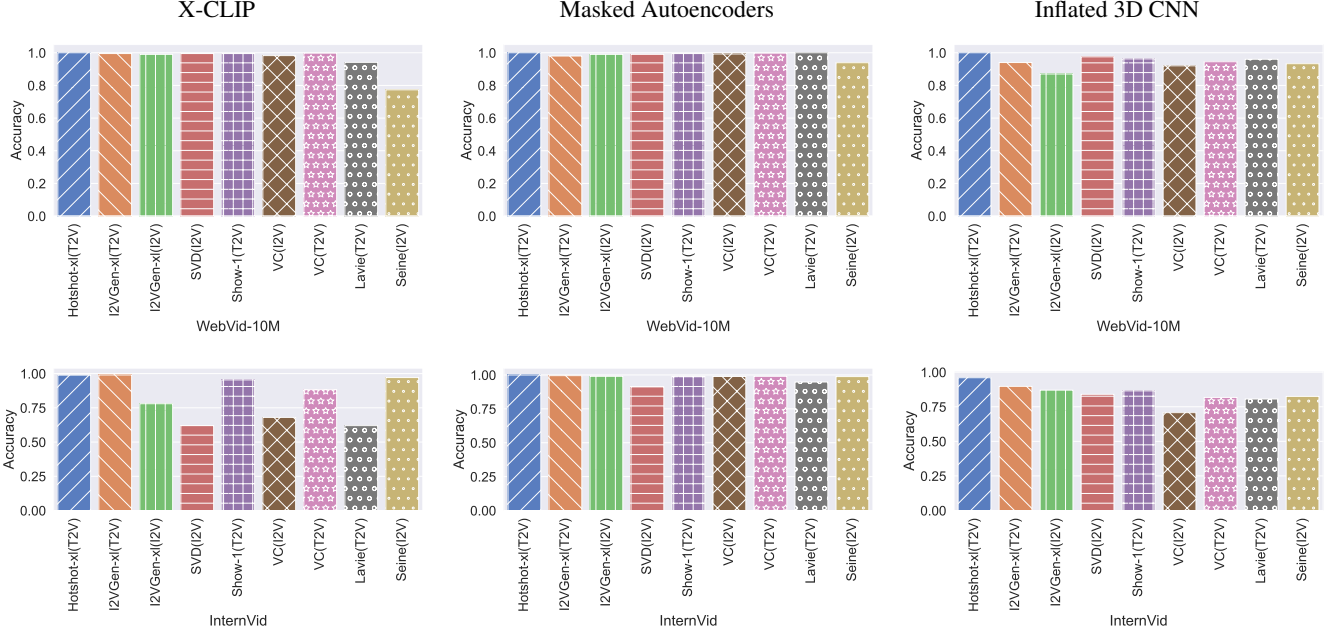


Figure 3: From left to right, the models utilize X-CLIP [36], MAE [54], and I3D [8] as backbones for constructing detection models. The first row presents detection results for synthesized videos using data from WebVid [1], while the second row features videos generated with the InternVid [62].

ably, the detection model built using X-CLIP [36] exhibited only nearly 62% success rate in several tasks, especially in detecting videos produced by the SVD [3]. This marks a substantial decline in detection efficacy using X-CLIP on the InternVid dataset, as opposed to the WebVid dataset. A similar trend of noticeable reduction was observed in the detection model based on I3D [8] when applied to videos generated from the InternVid dataset. However, the detection model constructed with MAE maintained a relatively stable performance, approaching 100% effectiveness without a significant decrease. This is primarily due to the cross-frame attention mechanism in MAE, which might deliver more information than the 3D CNN architecture. Additionally, the total parameters of I3D are much lower than that of MAE model, which also impacts the model’s performance to some extent.

A comparative analysis of three distinct detection models reveals that the MAE [54] achieves the most effective detection performance with the highest stability in accuracy. This observation implies that detection accuracy might correlated with the amount of video information processed. Due to X-CLIP’s [36] limitation in processing a smaller number of video frames, its detection efficacy is restricted. Both MAE and I3D [8], capable of processing 16 frames, access more extensive video information, thereby enhancing the precision of detection. However, a longitudinal comparison using the InternVid dataset [62] for video generation indicates a noticeable decline in the detection accuracy of the I3D model, particularly in several image-to-video generation tasks. This

Table 4: MAE-based fake video detection on four settings using the InternVid dataset [62].

Scenario	Targeted detection	M-blind	D-blind	Open detection
Hotshot-x1 (T2V)	0.99	0.95	1	–
I2V (T2V)	0.995	0.94	0.99	–
I2V (I2V)	0.99	–	0.82	–
SVD (I2V)	0.912	0.59	0.71	0.59
Show-1 (T2V)	0.99	0.72	0.94	–
VC (I2V)	0.989	0.65	0.80	–
VC (T2V)	0.99	0.62	0.92	–
Lavie (T2V)	0.948	0.58	0.62	0.73
Seine (I2V)	0.988	0.89	0.97	–

trend underscores the inherent instability of the I3D model as a detection mechanism, especially in capturing fine details in videos. It struggles with high-resolution image-induced generation tasks, potentially leading to detection failures. In contrast, MAE consistently maintains a stable detection accuracy, surpassing 90% across 18 tasks.

Untargeted Detection. We then focus on utilizing MAE-based detection model evaluate on InternVid dataset [62] and show results in Table 4. We observe that the detection model trained on fake videos generated by I2VGen-x1 (I2V) [67] exhibits the highest accuracy in *targeted detection*. Thus, this model is utilized in *M-blind* setting to individually assess videos from other generative tasks. It is distinctly noted that the detection model’s effectiveness significantly declines in tasks such

as SVD (I2V) [3], VC (I2V) [10], VC (T2V) [10], and Lavie (T2V) [61]. With a notable drop of up to 37% in VC (T2V) and Lavie (T2V). This suggests that the video characteristics inherent in the fake videos produced by I2VGen-x1 (I2V) differ from those generated by these tasks. Furthermore, the MAE-based detector effectively identifies fake videos generated by other tasks. This ability to discern model ‘fingerprints’ in generated videos underscores MAE’s potential in fulfilling real-world detection tasks.

D-blind involves using detection models trained on fake videos generated from the same models but querying from another dataset. While the detection accuracy of some tasks, such as SVD (I2V) [3] and Lavie (T2V) [61], shows a decline, the overall accuracy remains significantly higher compared to *M-blind*. From the results presented in Table 4, we observe that unknown generative models pose a more significant challenge compared with *D-blind*.

For *open detection*, we train a detection model using fake videos from all generation tasks (generated with WebVid dataset) except SVD (I2V) [3] and Lavie (T2V) [61]. This detection scenario encompasses the unknown generator aspect of *M-blind* and the unknown data source element of *D-blind*. Our focus is on SVD (I2V) [3] and Lavie (T2V) [61], both are queried from the InternVid dataset [62]. As previous results indicate their detection heavily relies on the uniformity of the data source and consistency of the generative model.

Contrary to our expectations, the detection accuracies of SVD (I2V) [3] and Lavie (T2V) [61] did not diminish with the reduction of known information. SVD (I2V) maintained a consistent accuracy rate comparable to that of *M-blind*. Meanwhile, Lavie (T2V) surpassed the accuracy rates of both *M-blind* and *D-blind*, achieving 72%. The higher success rate achieved by *Open detection* can be attributed to its exposure to a broader range of fake videos during training, compared to *M-blind* and *D-blind*. This extensive exposure allows the detection model to understand fake videos better, facilitating more effective detection.

Takeaways: In this section, we explore four attack scenarios based on awareness of data sources and generation models. *Targeted detection* proves the model’s proficiency in accurately recognizing fake videos. *D-blind* results show that fake videos generated by the same model but with different datasets share detectable ‘fingerprints’. *M-blind* findings reveal that videos from different models but similar data sources possess distinguishable features. Lastly, *open detection* demonstrates our method’s effectiveness, being data-independent and model-agnostic, capable of differentiating fake videos across various generative models. It can accurately identify fake videos from any production model with sufficient training data.

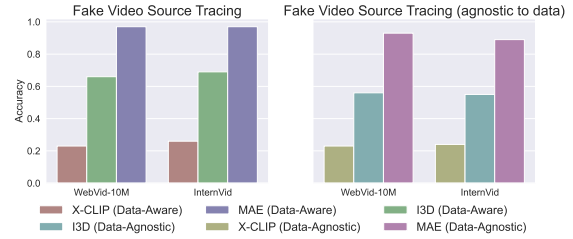


Figure 4: The results of source tracing under *data-aware* and *data-agnostic* settings on Webvid and InternVid datasets.

3.3.3 Source Tracing

Data-Aware Setting. In *data-aware* setting source tracing tasks, the primary focus is on assessing the model’s capability to detect ‘fingerprints’ contained in fake videos generated by various generative models. However, capturing the generative characteristics of these models, both temporally and spatially, highly depends on the length of the input video. Figure 4 demonstrates that the source tracing model utilizing X-CLIP [36] as its backbone fails to achieve satisfactory source tracing accuracy on two datasets, achieving only 24% and 26% accuracy, respectively. These accuracy levels are comparable to random guessing (11%) and indicate a lack of effective performance. We think that is because X-CLIP is limited to processing only eight frames of video data for feature collection. This undoubtedly presents more challenges compared to I3D and MAE. In contrast, the I3D-based source tracing model significantly outperforms X-CLIP, achieving an accuracy rate of over 60%. This improvement could be attributed to the ability of I3D [8] to process more (double) frames compared to X-CLIP, aiding in better judgment. The MAE-based source tracing model stands out for its stable and superior performance. With an understanding of the data distribution, source tracing using MAE [54] can reach an impressive 97% accuracy rate on two datasets.

Data-Agnostic Setting. Even in scenarios where the data source of the generated videos is uncertain, the MAE-based source tracing model still achieves an accuracy of 90%. Although this represents a slight decline from the source tracing accuracy in *data-aware* setting, it is less than a 10% decrease. This performance still significantly surpasses the X-CLIP- and I3D-based source tracing models, which have detection accuracy of only 20% and 50%, respectively.

We attribute this to MAE’s ability to discern the distinct ‘signatures’ carried by videos generated from different video generation tasks, as proposed in Section 3.2.2. Therefore, the MAE-based source tracing model possesses the capability to perform tracing tasks of fake videos in an open-world context.



Figure 5: Employing Grad-CAM [48] to demonstrate the specific aspects of the video that inform the detection decision-making process. Case study on generated samples from InternVid [62] shows that I3D-based detection model focuses on a few pixels and will not move to another region. The MAE-based detection model will be more flexible and capable of focusing on different anomalous objects across various frames. Furthermore, the MAE-based detection can identify anomalies through the trajectories of motion and shape of objects across temporal dimensions.

Takeaways: Our experimental results demonstrate that the source tracing model using MAE as its backbone exhibits superior performance, achieving a 90% accuracy rate in source tracing under agnostic data conditions. Our designed model can trace the source accurately using the generative model’s features on its generated videos, without considering the data source.

3.4 Analysis via Grad-CAM

3.4.1 Detection

Observing that both detection models build on I3D [8] and MAE [54] achieve an accuracy exceeding 90% in Figure 3. We were intrigued by the reasons behind the model’s high detection performance. Further, we observed differences in detection effectiveness between two distinct backbone detection models. Therefore, we investigated the underlying factors that enable the models to accurately distinguish between authentic and generated videos.

Our goal is to explore the criteria detection models used to distinguish fake videos, considering their temporal and spatial features. Also, we aim to uncover the factors contributing to the varying detection accuracy levels observed when analyzing fake videos. Towards this goal, we employ Grad-CAM [48] on the detection models to dissect the bases of their judgments. Figure 5 only illustrates a single frame of a video generated using Grad-CAM with two detection models for the InternVid-SVD generation task. The complete video

with heatmaps is shown in Appendix C. A common characteristic of the I3D-based and MAE-based detection models is that their judgments predominantly rely on the objects within the videos. For example, as illustrated in Figure 6, Grad-CAM reveals that the I3D-based detection model primarily focuses on human faces, fences, fingers, and engine batteries, while the MAE-based model concentrates on sewer covers, human bodies, and fingers. Both models under our investigation are adept at identifying these deformed objects in the videos. This is attributed to the current challenges of video generation models in accurately reconstructing objects, leading to distortions and twisting in spatial dimensions.

As for temporal level detection, a notable difference is observed in their ‘focus stability’. For instance, as seen in the second image of the first column in Figure 5, the I3D-based detection model [8] consistently focuses on the left fence area. While it does observe people in the scene in later frames, it is not as sensitive as the MAE-based detection model. In the same video, the MAE-based detection model initially focuses on the left fence but quickly shifts its attention to the anomalously rendered human figure. Mainly, it notices the distorted legs, a deviation that the MAE-based model promptly detects.

In another video, exemplified by the top image in the third column of Figure 5. The MAE-based detection model zeroes in on anomalies at the white drain. Initially, the MAE-based detection model does not perceive anything unusual. However, as the generated video drastically alters the drain’s layout – changing from orderly to distorted between frames – the MAE-based detection model detects this temporal inconsistency and focuses on this area. Moreover, it pays attention to anomalous changes in water ripples between frames, ultimately classifying the video as fake. Conversely, the I3D-based detection model’s capacity to scrutinize temporal anomalies is less robust than the MAE-based detection model. It fails to notice the significantly deformed drain between frames and the changes in water ripples. These experimental results suggest that compared to the MAE-based detection model, the I3D-based detection model struggles to detect temporal abnormalities. It predominantly bases its judgments on anomalously reconstructed objects by video generation models.

We recognize that this explains why the I3D-based [8] detection model exhibits a lower detection accuracy than the MAE-based detection model. As video generation models evolve and gain proficiency in object reconstruction, the I3D-based detection model might need help identifying fake videos with solely spatial anomalies.

Takeaways: The I3D-based detection model primarily relies on identifying objects’ spatial distortions to determine a video’s authenticity. Its focus points within the video are relatively fixed, lacking the capacity to comprehend abnormal changes in the temporal space. In contrast, the MAE-based detection model is more



Figure 6: Fake video source tracing model relies on detecting characteristics at different positions in the video to determine the generating model.

versatile in detecting anomalies. It not only observes spatial distortions of objects but also pays attention to unusual movements of objects between the current and previous frames.

3.4.2 Source Tracing

Consistent with Section 3.4.1, we continue to delve further. We explore what attributes of fake videos the source tracing model relies upon to identify the model that generated them. To this end, because the data sample from InternVid dataset [62] have higher resolution, we queried I2VGen-xl [67], VideoCrafter [10], Stable Video Diffusion [3], and Seine [11] using previously unused data from it. We employed an I3D-based source tracing model to infer the generative models of these fake videos. After confirming the ability of the source tracing model to track the generative models of these four videos, we reapplied the Grad-CAM [48] again. Our objective was to discern which areas of the videos were observed by the model to make its determinations. In Figure 6, we present selected frames from the source tracing task, illustrating that the source tracing model focuses on different aspects of videos generated by different models. For instance, in videos generated by Stable Video Diffusion [3], the tracing model bases its judgment on the upper body of the generated human figures. In contrast, for the I2VGen-xl [67], the source tracing model pays more attention to the background generation effects behind the human figure. We discovered that, like humans, the source tracing model has the capability to recognize specific styles in certain objects generated by different models to aid in its judgment. For example, human figures generated by Stable Video Diffusion tend to be more distorted, while backgrounds generated by I2VGen-xl are more blurred. This finding also substantiates our source tracing model’s agnostic-to-data capability, enabling it to make determinations based on features con-

tained within the generated videos rather than being confined to detecting only from specific data sources.

Takeaways: Videos generated from the same image by different models will contain unique characteristics specific to each model. For instance, features such as the misshapen generated human figures or the blurriness of backgrounds are specific to individual models. These characteristics can assist the source tracing model in effectively tracing the origin of the videos. Moreover, these features are agnostic to data sources.

4 Misuse Prevention

Compared to text-to-video generation tasks, videos produced through image-to-video generation tasks are more susceptible to abuse due to the existence of Modifier. They are more likely to lead to copyright infringement and misuse issues. At the same time, with the development of video generation models, fake videos might be more time-coherent and have a higher resolution. Therefore, only employing fake video detection in such scenarios may not be enough. A dedicated defensive strategy is needed for this type of generation tasks. We plan to design a defense mechanism based on the concept of *adversarial examples*, tailored explicitly for the image-to-video generation task.

Adversarial examples are first introduced to target misclassification problems, incorporating a small perturbation to the original image but are invisible to humans [6, 17, 32, 37, 40, 43, 55]. Szegedy et al. [53] first proposed the concept of adversarial samples. Their work narrates how adding perturbations to an image can lead to incorrect judgments by neural networks. Following this, methods for generating adversarial examples, such as FGSM [17], C&W [7], and PGD [37], emerged. Early adversarial examples were primarily used in classification models, aiming to confuse classifiers to elicit incorrect cate-

gorization results. In our task, we aim to confuse video generative models, and hence, we employ a method similar to PGD [37] to create adversarial examples for defense.

Our intuition is video generation models utilize encoders to analyze objects within the input images. For instance, as demonstrated in Figure 7, if the image contains a rocket, the model discerns the object in the image and generates corresponding continuous frames, ultimately stringing these frames together to create a video. Thus, it is necessary to deceive the model’s encoder into misinterpreting the image, thereby producing incorrect and bizarre frames, ultimately safeguarding the image from misuse.

4.1 Methodology

We use $E_1(\cdot)$ to denote the model’s understanding of the image in the spatial domain, and $E_2(\cdot)$ for its understanding in the temporal domain. We introduced a directed defense approach and an undirected one; they are different in that the directed approach needs the `Creator` to pick a target image \tilde{x} and the undirected does not. We will provide a detailed discussion of these two methods in the following.

Directed Defense. The method of *directed defense* involves using a guiding image to direct the perturbations added to x , which we refer to as the target image \tilde{x} . Our aim is for the modified image \hat{x} to be similar to the original image x at the pixel level while resembling \tilde{x} at the semantic level. Accordingly, we have crafted our optimization objective as follows:

$$\begin{aligned} \arg \min_{\hat{x}} & \|E_1(\hat{x}) - E_1(\tilde{x})\|_{\ell_1} + \lambda_1 \cdot \|E_2(\hat{x}) - E_2(\tilde{x})\|_{\ell_1} \\ & + \lambda_2 \cdot [\|\hat{x} - x\|_{\ell_2} + L_{\text{lips}}(\hat{x}, x)] \end{aligned} \quad (4)$$

Herein, we desire the generated adversarial example \hat{x} to attain a similar semantic understanding when processed by the E_1 and E_2 encoders. This calculation will employ either the L_1 norm or cosine similarity matrix. Concurrently, we use the L_2 norm and L_{lips} loss between \hat{x} and x to ensure similarity at the pixel level.

Algorithm 1 Directed Defense

Input: Original image x , target image \tilde{x} , image encoder E_1 , video encoder E_2 , optimization rate μ , upper bound η , number of iterations T

- 1: Utilizing objection function as defined in Equation 4
- 2: Set the initial adversarial example $\hat{x}_0 \leftarrow x$
- 3: **for** $i \leftarrow 0$ **to** $T - 1$ **do** \triangleright Perform T repetitive iterations.
- 4: $\hat{x}_i^* \leftarrow \hat{x}_i - \mu \cdot \text{sgn}(\nabla_{\hat{x}_i} L(\hat{x}_i, \tilde{x}, E_1, E_2))$
- 5: $\beta \leftarrow \hat{x}_i^* - x$ and bound $\beta \leq \|\eta\|_{\ell_1}$
- 6: $\hat{x}_{i+1} \leftarrow x + \beta$
- 7: **end for**

Output: \hat{x}_T \triangleright \hat{x}_T simplify denoted as \hat{x} in our paper

Theoretically, we can take any off-the-shelf optimizer to find \hat{x} . In our setting, we apply a PGD-style method, as shown in Algorithm 1. Specifically, we compute the loss for each iteration using the loss function from Equation 4, and after calculating the derivative, we subtract this gradient value from the current iteration’s \hat{x}^i . This is because our *directed defense* is formulated as an optimization problem aimed at approximating the target image’s projections $E_1(\cdot)$ and $E_2(\cdot)$, thereby necessitating the application of gradient descent. We treat η as hyperparameters in our experiments, and we will evaluate them in Section 4.2.1.

Undirected Defense. The target image \tilde{x} substantially influences the efficacy of *directed defense*. Careful selection of the target image is imperative to achieve optimal defensive outcomes. However, this selection process often necessitates semantic and pixel filtering, which varies depending on the original image. To obviate the laborious task of selecting target images for each unique original image, we propose our *undirected defense* method. This allows for the implementation of defense strategies irrespective of the original image.

$$\begin{aligned} \arg \max_{\hat{x}} & \|E_1(\hat{x}) - E_1(x)\|_{\ell_1} + \lambda_1 \cdot \|E_2(\hat{x}) - E_2(x)\|_{\ell_1} \\ & - \lambda_2 \cdot [\|\hat{x} - x\|_{\ell_2} + L_{\text{lips}}(\hat{x}, x)] \end{aligned} \quad (5)$$

We posit that the adversarial example \hat{x} requires iterative modifications to increase its distance from x in the latent space projected by $E_1(\cdot)$ and $E_2(\cdot)$. We employ the L_1 norm to measure the distance between embeddings and iteratively optimize \hat{x} . Similar to *directed defense* strategies, our optimization process also aims to maintain proximity to the original image x . To this end, we opt for the use of L_{lips} and L_2 norm to control pixel-level similarity. The objective function of *undirected defense* is defined in Equation 5.

The primary distinction between *directed defense* and *undirected defense* lies in three aspects. First is eliminating the need for a target image \tilde{x} . Second, there is the use of a different objective function. Third, a modification occurs in the computation sign at line 4 in Algorithm 1. The *undirected defense* transforms the method into a maximization optimization problem. Similar to traditional methods of generating adversarial examples [17], our objective is to add perturbations that amplify the loss in $E_1(\cdot)$ and $E_2(\cdot)$, effectively achieving a gradient ascent, hence the utilization of the addition sign.

4.2 Evaluation

In this section, our experiments encompass not only open-source models capable of supporting image-to-video generation, such as SVD [3], but we will also conduct tests on several commercial models referenced in Section 2.1 to further substantiate the effectiveness of our approach.

We will adopt the original adversarial strategy against image generation as the baseline method [33, 50], which pri-

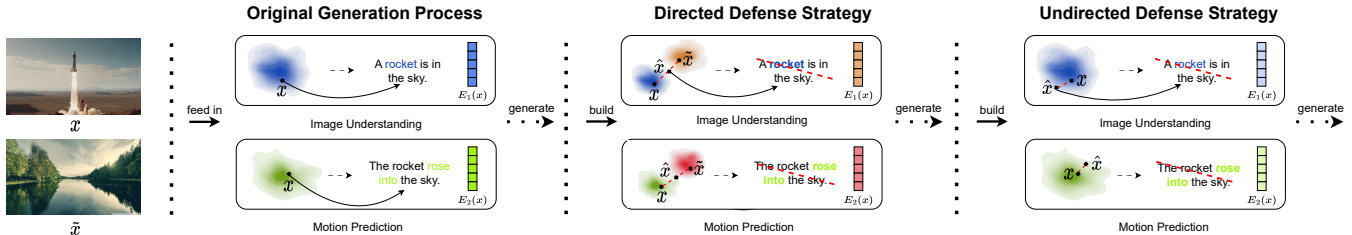


Figure 7: Prevention strategies are implemented by introducing perturbations to x , causing semantic shifts. *Directed defense* employs a selectively chosen \tilde{x} for guidance, while *undirected defense* adds perturbations indiscriminately.

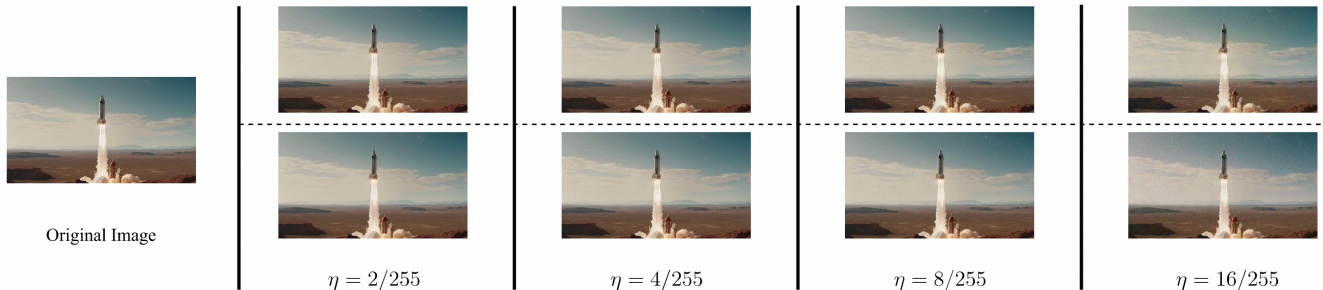


Figure 8: Adversarial examples with $\eta = \frac{2}{255}, \frac{4}{255}, \frac{8}{255},$ and $\frac{16}{255}$, the first row applies a *directed defense* method, and the second row an *undirected defense* method.

marily focuses on object understanding and overlooks motion prediction in the image. We use two embedders from SVD [3] in our experiments. E_1 , the first-layer embedder, is the ‘FrozenOpenCLIPImagePredictionEmbedder’⁹. It generates embeddings for conditional frames. E_2 , the fourth-layer embedder, is the ‘VideoPredictionEmbedderWithEncoder’¹⁰. It creates inputs for UNet, aiming for temporal-level prediction. The parameters λ_1 and λ_2 are both set to 1 in Equation 4 and Equation 5. μ is set to $\frac{1}{255}$, as this configuration has demonstrated effective defense capabilities.

4.2.1 Directed Defense

This section showcases the adversarial examples created using Algorithm 1 in Figure 8. We have set four distinct levels of η values for testing, specifically at $\eta = \frac{2}{255}, \frac{4}{255}, \frac{8}{255},$ and $\frac{16}{255}$. As observed from the output image, due to the requirement of a target image \tilde{x} as a guide in Algorithm 1, the generated \hat{x} also incorporates imprints from \tilde{x} . We aim to add invisible perturbations for defense purposes; hence, we limited the range of added perturbations to a maximum of $\frac{16}{255}$. The images in Figure 10a reveal that setting η to $\frac{4}{255}$ affects the videos generated by Stable Video Diffusion [3]. The rocket in the scene exhibits erroneous motion prediction, remaining stationary in mid-air. At the same time, the background clouds

⁹CLIP image encoder server as the ‘FrozenOpenCLIPImagePredictionEmbedder’ in Stable Video Diffusion.

¹⁰Stable Diffusion 2.1 encoder is utilized as the ‘VideoPredictionEmbedderWithEncoder’ in Stable Video Diffusion.

continue to move, indicating a temporal anomaly in object motion. However, in contrast to the baseline method that adds perturbations only at the semantic level, we found that even with $\eta = \frac{16}{255}$, it fails to disrupt video generation process effectively. The model still retains the ability to comprehend the objects in the image and generate videos based on the motion of the target objects.

Furthermore, as shown in Figure 10b, we also tested our $\eta = \frac{8}{255}$ adversarial example on other video generation models. When targeted on Gen-2, we have observed a significant difference. Compared to videos generated from images without added perturbation, those created from adversarial examples using Algorithm 1 successfully disrupt the rocket’s motion. Although smoke continues to emanate from the bottom of the rocket, it remains stationary in mid-air, effectively compromising the motion generation aspect of the video. Given that the videos generated by Pika Lab from the original images feature only subtle movements of the rocket, we did not observe any significant motion anomalies for the rocket. However, the smoke emitted from the rocket is static.

4.2.2 Undirected Defense

The *undirected defense* method does not require the guidance of a target image but instead directly optimizes the image to increase the loss. We observed in Figure 8 that at $\eta = \frac{16}{255}$, the adversarial example generated by the *undirected defense* method appears more similar to the original image. This is compared to that generated by the *directed defense* method,

Table 5: The defensive effectiveness of adversarial examples with four varying levels of perturbation intensity was evaluated on Stable Video Diffusion, Gen-2, and Pika Lab.

	SVD				Gen-2				Pika Lab			
	$\frac{2}{255}$	$\frac{4}{255}$	$\frac{8}{255}$	$\frac{16}{255}$	$\frac{2}{255}$	$\frac{4}{255}$	$\frac{8}{255}$	$\frac{16}{255}$	$\frac{2}{255}$	$\frac{4}{255}$	$\frac{8}{255}$	$\frac{16}{255}$
Baseline (directed)	✗	✗	✗	✗	✗	✗	✗	✓	✗	✗	✗	✗
Baseline (undirected)	✗	✗	✗	✗	✗	✗	✗	✓	✗	✗	✗	✗
Ours (directed)	✗	✓	✓	✓	✗	✓	✓	✓	✗	✗	✓	✓
Ours (undirected)	✗	✓	✓	✓	✗	✗	✓	✓	✗	✗	✗	✓

as seen in the first row. In the upper left sky portion of two images, the *directed defense* method introduces certain features from the target image. Meanwhile, the *undirected defense* maintains more visual similarity and equivalent defense effectiveness. The images in Figure 10a show that the *undirected defense* method is effective. Even at $\eta = \frac{4}{255}$, it can successfully prevent Stable Video Diffusion [3] from generating reasonable videos. The rocket remains stationary in the air, which leads to incorrect motion prediction by the model. We also applied the baseline method [33, 50] using the *undirected defense* procedure. Similar to findings in Section 4.2.1, we found that merely disrupting the semantic understanding of the image without affecting object motion is insufficient for effective defense.

Similarly, we utilized adversarial examples generated by the *undirected defense* as inputs for experimentation with Pika Lab and Gen-2. On Gen-2, we observed the rocket’s motion, which did not significantly differ from the original video. However, the video generated from images processed by *undirected defense* exhibited distorted and anomalous motion in the rocket’s launch base, increasing the video’s implausibility. In contrast, videos generated on Pika Lab were akin to the original unaltered videos, with no noticeable differences in objects or dynamics.

4.3 Discussion

The results of each defense method under four different η settings can be observed in Table 5. We have found that both proposed methods effectively prevent Stable Video Diffusion [3] from generating regular videos. However, our approach faces a limitation since we utilized the image and video encoders of Stable Video Diffusion in *directed defense* and *undirected defense*. When dealing with unknown video generation models, the adversarial examples generated by the *directed defense* method would have weaker preventive capabilities.

Compared with *undirected defense*, *directed defense* strategy can provide more effective defense. The effectiveness of this approach stems from directing images in the latent space toward that of another image. Thus, it enhances the potential to deceive the video generation model, leading to misinterpreting the input image. As a trade-off, *directed defense* may introduce more features from the target image, potentially impacting the image quality when the value of

η is large. Therefore, choosing an appropriate target image becomes crucial. The selected target image should overlap substantially with the scene of the original image while having differences in the main object. Such *directed defense* ensures the invisibility of the perturbation.

Takeaways: Both directed and undirected defenses can effectively provide invisible protection to images. Moreover, *directed defense* is not only effective against Stable Video Diffusion but also causes disruption in videos generated using Gen-2 and Pika Lab models.

5 Related Work

5.1 Fake Content Detection

With the advancement of generative models, researchers have identified the security issues they entail. These include creating fake images and generating misleading audio based on conditional prompt input. Notably, an increasing number of researchers are investigating and analyzing the outputs generated by AI models. Their focus is on visual media such as images and videos [2, 12, 13, 15, 16, 20, 23, 35, 49, 57, 58, 63, 65, 68, 73], audio [44, 56] and text [31, 38]. In the image generation domain, these efforts have been made to discriminate between images produced by GANs and advanced text-to-image diffusion models [49, 58, 65]. Likewise, in the domains of audio synthesis [44, 56] and text generation [31, 38], the challenges are distinct. Due to differences in generation tasks and the variety of generative models, existing methods cannot be directly applied to safeguard privacy in video generation models.

In the realm of fake video detection, several existing works are focused on the fundamental video generation models, which cannot synthesize high resolution and diversity output [13, 15, 20, 23, 57, 63]. All of these methods are detect videos generated by GANs and it is primarily focused on face swap videos. The content is fixed, and due to the performance of video generators, the distinction between real and fake videos is pronounced.

5.2 Video Diffusion Models

Earlier video diffusion models predominantly operated the diffusion process in the pixel space [25, 27, 52]. Due to computational intensity and limitations in training data, such models struggled to generate high-resolution and coherent videos. However, with growing demands for higher resolution in generated videos and considerations of computational resources during runtime, latent diffusion models have been proposed [3, 4, 10, 11, 24, 61, 66, 67, 72]. These latent diffusion models significantly alleviate computational performance issues and often utilize a framework akin to Stable

Diffusion [47], albeit augmented with temporal layers. Based on the input provided by users, video generation tasks can be divided into text-to-video and image-to-video categories.

6 Conclusion

Our work is mainly targeting misuse problems in video generation models. We begin by defining the roles present in the real-world setting and, subsequently, design three methods to address misuse issues. Both the detection, source tracing, and prevention tasks utilize the anomalies of spatial-temporal dynamics within the fake videos. Our proposed methods constitute a comprehensive defense pipeline, effectively countering current state-of-the-art video generation models.

There are some limitations: The *fake video detection* models and *fake video source tracing* models achieve high accuracy by leveraging features attributed to spatial and temporal spaces. However, the evolution of video generation models (i.e., Sora) will enable the production of more time-consistent and reasonable videos. Our methods may require refinement to detect and trace sources of such advanced fake videos. While the defensive strategies we propose offer effective protection, *directed defense* needs the selection of an appropriate target image for guidance. Conversely, the *undirected defense* may require a larger η value for similar defensive effects without needing guidance. Finally, exploring the abuse concern of the *video modification models* is a different task and is not described in our paper.

References

- [1] BAIN, M., NAGRANI, A., VAROL, G., AND ZISSERMAN, A. Frozen in time: A joint video and image encoder for end-to-end retrieval. In *IEEE International Conference on Computer Vision* (2021).
- [2] BIRD, J. J., AND LOTFI, A. Cifake: Image classification and explainable identification of ai-generated synthetic images, 2023.
- [3] BLATTMANN, A., DOCKHORN, T., KULAL, S., MENDELEVITCH, D., KILIAN, M., LORENZ, D., LEVI, Y., ENGLISH, Z., VOLETI, V., LETTS, A., JAMPANI, V., AND ROMBACH, R. Stable video diffusion: Scaling latent video diffusion models to large datasets, 2023.
- [4] BLATTMANN, A., ROMBACH, R., LING, H., DOCKHORN, T., KIM, S. W., FIDLER, S., AND KREIS, K. Align your latents: High-resolution video synthesis with latent diffusion models, 2023.
- [5] BONETTINI, N., CANNAS, E. D., MANDELLI, S., BONDI, L., BESTAGINI, P., AND TUBARO, S. Video face manipulation detection through ensemble of cnns, 2020.
- [6] CARLINI, N., AND WAGNER, D. Towards evaluating the robustness of neural networks, 2017.
- [7] CARLINI, N., AND WAGNER, D. Towards evaluating the robustness of neural networks. In *2017 IEEE Symposium on Security and Privacy (SP)* (2017), Ieee, pp. 39–57.
- [8] CARREIRA, J., AND ZISSERMAN, A. Quo vadis, action recognition? a new model and the kinetics dataset, 2018.
- [9] CEYLAN, D., HUANG, C.-H. P., AND MITRA, N. J. Pix2video: Video editing using image diffusion, 2023.
- [10] CHEN, H., XIA, M., HE, Y., ZHANG, Y., CUN, X., YANG, S., XING, J., LIU, Y., CHEN, Q., WANG, X., WENG, C., AND SHAN, Y. Videocrafter1: Open diffusion models for high-quality video generation, 2023.
- [11] CHEN, X., WANG, Y., ZHANG, L., ZHUANG, S., MA, X., YU, J., WANG, Y., LIN, D., QIAO, Y., AND LIU, Z. Seine: Short-to-long video diffusion model for generative transition and prediction, 2023.
- [12] COZZOLINO, D., NAGANO, K., THOMAZ, L., MAJUMDAR, A., AND VERDOLIVA, L. Synthetic image detection: Highlights from the ieeec video and image processing cup 2022 student competition, 2023.
- [13] DANG, H., LIU, F., STEHOUEW, J., LIU, X., AND JAIN, A. On the detection of digital face manipulation, 2020.
- [14] ESSER, P., CHIU, J., ATIGHEHCHIAN, P., GRANSKOG, J., AND GERMANIDIS, A. Structure and content-guided video synthesis with diffusion models, 2023.
- [15] GANDHI, A., AND JAIN, S. Adversarial perturbations fool deepfake detectors, 2020.
- [16] GIRISH, S., SURI, S., RAMBHATLA, S., AND SHRIVASTAVA, A. Towards discovery and attribution of open-world gan generated images, 2021.
- [17] GOODFELLOW, I. J., SHLENS, J., AND SZEGEDY, C. Explaining and harnessing adversarial examples, 2015.
- [18] GU, Z., CHEN, Y., YAO, T., DING, S., LI, J., HUANG, F., AND MA, L. Spatiotemporal inconsistency learning for deepfake video detection. In *Proceedings of the 29th ACM international conference on multimedia* (2021), pp. 3473–3481.
- [19] GU, Z., CHEN, Y., YAO, T., DING, S., LI, J., AND MA, L. Delving into the local: Dynamic inconsistency learning for deepfake video detection. In *Proceedings of the AAAI Conference on Artificial Intelligence* (2022), vol. 36, pp. 744–752.
- [20] GÜERA, D., AND DELP, E. J. Deepfake video detection using recurrent neural networks. In *2018 15th IEEE International Conference on Advanced Video and Signal Based Surveillance (AVSS)* (2018), pp. 1–6.
- [21] HA, A. Y. J., PASSANANTI, J., BHASKAR, R., SHAN, S., SOUTHEN, R., ZHENG, H., AND ZHAO, B. Y. Organic or diffused: Can we distinguish human art from ai-generated images?, 2024.
- [22] HE, K., CHEN, X., XIE, S., LI, Y., DOLLÁR, P., AND GIRSHICK, R. Masked autoencoders are scalable vision learners, 2021.
- [23] HE, Y., GAN, B., CHEN, S., ZHOU, Y., YIN, G., SONG, L., SHENG, L., SHAO, J., AND LIU, Z. Forgerynet: A versatile benchmark for comprehensive forgery analysis, 2021.
- [24] HE, Y., YANG, T., ZHANG, Y., SHAN, Y., AND CHEN, Q. Latent video diffusion models for high-fidelity long video generation, 2023.
- [25] HO, J., CHAN, W., SAHARIA, C., WHANG, J., GAO, R., GRITSENKO, A., KINGMA, D. P., POOLE, B., NOROUZI, M., FLEET, D. J., AND SALIMANS, T. Imagen video: High definition video generation with diffusion models, 2022.
- [26] HO, J., JAIN, A., AND ABBEEL, P. Denoising diffusion probabilistic models, 2020.
- [27] HO, J., SALIMANS, T., GRITSENKO, A., CHAN, W., NOROUZI, M., AND FLEET, D. J. Video diffusion models, 2022.
- [28] HU, Z., XIE, H., WANG, Y., LI, J., WANG, Z., AND ZHANG, Y. Dynamic inconsistency-aware deepfake video detection. In *IJCAI* (2021), pp. 736–742.
- [29] JI, S., XU, W., YANG, M., AND YU, K. 3d convolutional neural networks for human action recognition. *IEEE transactions on pattern analysis and machine intelligence* 35, 1 (2012), 221–231.
- [30] KARIM, N., KHALID, U., JONEIDI, M., CHEN, C., AND RAHNAVARD, N. Save: Spectral-shift-aware adaptation of image diffusion models for text-driven video editing, 2023.

- [31] KRISHNA, K., SONG, Y., KARPINSKA, M., WIETING, J., AND IYER, M. Paraphrasing evades detectors of ai-generated text, but retrieval is an effective defense. *arXiv preprint arXiv:2303.13408* (2023).
- [32] KURAKIN, A., GOODFELLOW, I., AND BENGIO, S. Adversarial examples in the physical world, 2017.
- [33] LIANG, C., WU, X., HUA, Y., ZHANG, J., XUE, Y., SONG, T., XUE, Z., MA, R., AND GUAN, H. Adversarial example does good: Preventing painting imitation from diffusion models via adversarial examples, 2023.
- [34] LIU, S., ZHANG, Y., LI, W., LIN, Z., AND JIA, J. Video-p2p: Video editing with cross-attention control, 2023.
- [35] LU, Z., HUANG, D., BAI, L., QU, J., WU, C., LIU, X., AND OUYANG, W. Seeing is not always believing: Benchmarking human and model perception of ai-generated images, 2023.
- [36] MA, Y., XU, G., SUN, X., YAN, M., ZHANG, J., AND JI, R. X-clip: End-to-end multi-grained contrastive learning for video-text retrieval, 2022.
- [37] MADRY, A., MAKELOV, A., SCHMIDT, L., TSIPRAS, D., AND VLADU, A. Towards deep learning models resistant to adversarial attacks, 2019.
- [38] MITCHELL, E., LEE, Y., KHAZATSKY, A., MANNING, C. D., AND FINN, C. Detectgpt: Zero-shot machine-generated text detection using probability curvature, 2023.
- [39] MOLAD, E., HORWITZ, E., VALEVSKI, D., ACHA, A. R., MATIAS, Y., PRITCH, Y., LEVIATHAN, Y., AND HOSHEN, Y. Dreamix: Video diffusion models are general video editors, 2023.
- [40] MOOSAVI-DEZFOOLI, S.-M., FAWZI, A., AND FROSSARD, P. Deepfool: a simple and accurate method to fool deep neural networks, 2016.
- [41] MULLAN, J., CRAWBUCK, D., AND SASTRY, A. Hotshot-XL, Oct. 2023.
- [42] NI, Y., MENG, D., YU, C., QUAN, C., REN, D., AND ZHAO, Y. Core: Consistent representation learning for face forgery detection, 2022.
- [43] PAPERNOT, N., MCDANIEL, P., JHA, S., FREDRIKSON, M., CELIK, Z. B., AND SWAMI, A. The limitations of deep learning in adversarial settings, 2015.
- [44] PRADHAN, S., SUN, W., BAIG, G., AND QIU, L. Combating replay attacks against voice assistants. *Proceedings of the ACM on Interactive, Mobile, Wearable and Ubiquitous Technologies* 3, 3 (2019), 1–26.
- [45] RADFORD, A., KIM, J. W., HALLACY, C., RAMESH, A., GOH, G., AGARWAL, S., SASTRY, G., ASKELL, A., MISHKIN, P., CLARK, J., KRUEGER, G., AND SUTSKEVER, I. Learning transferable visual models from natural language supervision, 2021.
- [46] REN, J., XU, H., HE, P., CUI, Y., ZENG, S., ZHANG, J., WEN, H., DING, J., LIU, H., CHANG, Y., AND TANG, J. Copyright protection in generative ai: A technical perspective, 2024.
- [47] ROMBACH, R., BLATTMANN, A., LORENZ, D., ESSER, P., AND OMMER, B. High-resolution image synthesis with latent diffusion models, 2022.
- [48] SELVARAJU, R. R., COGSWELL, M., DAS, A., VEDANTAM, R., PARIKH, D., AND BATRA, D. Grad-cam: Visual explanations from deep networks via gradient-based localization. *International Journal of Computer Vision* 128, 2 (Oct. 2019), 336–359.
- [49] SHA, Z., LI, Z., YU, N., AND ZHANG, Y. De-fake: Detection and attribution of fake images generated by text-to-image generation models, 2023.
- [50] SHAN, S., CRYAN, J., WENGER, E., ZHENG, H., HANOCKA, R., AND ZHAO, B. Y. Glaze: Protecting artists from style mimicry by text-to-image models, 2023.
- [51] SHIN, C., KIM, H., LEE, C. H., GIL LEE, S., AND YOON, S. Edit-a-video: Single video editing with object-aware consistency, 2023.
- [52] SINGER, U., POLYAK, A., HAYES, T., YIN, X., AN, J., ZHANG, S., HU, Q., YANG, H., ASHUAL, O., GAFNI, O., PARIKH, D., GUPTA, S., AND TAIGMAN, Y. Make-a-video: Text-to-video generation without text-video data, 2022.
- [53] SZEGEDY, C., ZAREMBA, W., SUTSKEVER, I., BRUNA, J., ERHAN, D., GOODFELLOW, I., AND FERGUS, R. Intriguing properties of neural networks, 2014.
- [54] TONG, Z., SONG, Y., WANG, J., AND WANG, L. Videomae: Masked autoencoders are data-efficient learners for self-supervised video pre-training, 2022.
- [55] TRAMÈR, F., PAPERNOT, N., GOODFELLOW, I., BONEH, D., AND MCDANIEL, P. The space of transferable adversarial examples, 2017.
- [56] VILLALBA, J., AND LLEIDA, E. Preventing replay attacks on speaker verification systems. In *2011 Carnahan Conference on Security Technology* (2011), IEEE, pp. 1–8.
- [57] WANG, R., JUEFEI-XU, F., MA, L., XIE, X., HUANG, Y., WANG, J., AND LIU, Y. Fakespotter: A simple yet robust baseline for spotting ai-synthesized fake faces, 2020.
- [58] WANG, S.-Y., WANG, O., ZHANG, R., OWENS, A., AND EFROS, A. A. Cnn-generated images are surprisingly easy to spot... for now, 2020.
- [59] WANG, W., YANG, H., TUO, Z., HE, H., ZHU, J., FU, J., AND LIU, J. Videofactory: Swap attention in spatiotemporal diffusions for text-to-video generation, 2023.
- [60] WANG, X., YUAN, H., ZHANG, S., CHEN, D., WANG, J., ZHANG, Y., SHEN, Y., ZHAO, D., AND ZHOU, J. Videocomposer: Compositional video synthesis with motion controllability, 2023.
- [61] WANG, Y., CHEN, X., MA, X., ZHOU, S., HUANG, Z., WANG, Y., YANG, C., HE, Y., YU, J., YANG, P., GUO, Y., WU, T., SI, C., JIANG, Y., CHEN, C., LOY, C. C., DAI, B., LIN, D., QIAO, Y., AND LIU, Z. Lavie: High-quality video generation with cascaded latent diffusion models, 2023.
- [62] WANG, Y., HE, Y., LI, Y., LI, K., YU, J., MA, X., LI, X., CHEN, G., CHEN, X., WANG, Y., HE, C., LUO, P., LIU, Z., WANG, Y., WANG, L., AND QIAO, Y. Internvid: A large-scale video-text dataset for multimodal understanding and generation, 2024.
- [63] WODAJO, D., ATNAFU, S., AND AKHTAR, Z. Deepfake video detection using generative convolutional vision transformer, 2023.
- [64] WU, J. Z., GE, Y., WANG, X., LEI, W., GU, Y., SHI, Y., HSU, W., SHAN, Y., QIE, X., AND SHOU, M. Z. Tune-a-video: One-shot tuning of image diffusion models for text-to-video generation, 2023.
- [65] YU, N., DAVIS, L., AND FRITZ, M. Attributing fake images to gans: Learning and analyzing gan fingerprints, 2019.
- [66] ZHANG, D. J., WU, J. Z., LIU, J.-W., ZHAO, R., RAN, L., GU, Y., GAO, D., AND SHOU, M. Z. Show-1: Marrying pixel and latent diffusion models for text-to-video generation, 2023.
- [67] ZHANG, S., WANG, J., ZHANG, Y., ZHAO, K., YUAN, H., QIN, Z., WANG, X., ZHAO, D., AND ZHOU, J. I2vgen-xl: High-quality image-to-video synthesis via cascaded diffusion models, 2023.
- [68] ZHANG, X., KARAMAN, S., AND CHANG, S.-F. Detecting and simulating artifacts in gan fake images, 2019.
- [69] ZHANG, Y., WEI, Y., JIANG, D., ZHANG, X., ZUO, W., AND TIAN, Q. Controlvideo: Training-free controllable text-to-video generation, 2023.
- [70] ZHAO, M., WANG, R., BAO, F., LI, C., AND ZHU, J. Controlvideo: Conditional control for one-shot text-driven video editing and beyond, 2023.
- [71] ZHAO, R., GU, Y., WU, J. Z., ZHANG, D. J., LIU, J., WU, W., KEPPO, J., AND SHOU, M. Z. Motiondirector: Motion customization of text-to-video diffusion models, 2023.

- [72] ZHOU, D., WANG, W., YAN, H., LV, W., ZHU, Y., AND FENG, J. Magicvideo: Efficient video generation with latent diffusion models, 2023.
- [73] ZHU, M., CHEN, H., YAN, Q., HUANG, X., LIN, G., LI, W., TU, Z., HU, H., HU, J., AND WANG, Y. Genimage: A million-scale benchmark for detecting ai-generated image, 2023.

A More Details for Diffusion Model

In this section, we want to discuss more details about the diffusion model. Since we have already explained what the diffusion process is in [Section 2](#). Therefore, In this part, we will mainly focus on the reverse (denoising) process. The reverse process can be described as:

$$p_{\theta}(x_{0:T}) = p(x_T) \prod_{t=1}^T p_{\theta}(x_{t-1}|x_t)$$

where $x_T \sim \mathcal{N}(0, I)$ and x_0 is the denoised image. For a step $t \in [0, T]$, the noise image x_{t-1} denoising from x_t can be represented as:

$$p_{\theta}(x_{t-1}|x_t) = \mathcal{N}(x_{t-1}; \mu_{\theta}(x_t, t), \Sigma_{\theta}(x_t, t))$$

The ground truth denoised image x_{t-1} can be sample from distribution $\mathcal{N}(x_{t-1}; \bar{\mu}(x_t, x_0), \bar{\beta}_t \mathbf{I})$. In DDPM [26], $\Sigma_{\theta}(x_t, t)$ is set to $\sigma_t^2 \mathbf{I}$ and is untrainable. Therefore, the diffusion model is mainly to approximate $\bar{\mu}(x_t, x_0)$ using $\mu_{\theta}(x_t, t)$. After applying Bayes’s rule to expend $\bar{\mu}(x_t, x_0)$. we can get

$$\bar{\mu}_t = \frac{\sqrt{\bar{\alpha}_t}(1 - \bar{\alpha}_{t-1})}{1 - \bar{\alpha}_t} x_t + \frac{\sqrt{\bar{\alpha}_{t-1}}(1 - \alpha_t)}{1 - \bar{\alpha}_t} \frac{1}{\sqrt{\bar{\alpha}_t}} (x_t - \sqrt{1 - \bar{\alpha}_t} \varepsilon_t) \quad (6)$$

Because we already have the ground-truth $\bar{\mu}_t$ the initial objective function can be written as:

$$L_t(\theta) = \mathbb{E}_{x_0, \varepsilon_t} \left[\|\bar{\mu}_t - \mu_{\theta}(\sqrt{\bar{\alpha}_t} x_0 + \sqrt{1 - \bar{\alpha}_t} \varepsilon_t, t)\|_2^2 \right] \quad (7)$$

In [Equation 6](#), we applied [Equation 1](#) to represent x_0 in $\bar{\mu}(x_t, x_0)$. The only term that is unknown and predictable is ε_t . Thus, $\mu_{\theta}(x_t, t)$ is reform as:

$$\mu_{\theta}(x_t, t) = \frac{\sqrt{\bar{\alpha}_t}(1 - \bar{\alpha}_{t-1})}{1 - \bar{\alpha}_t} x_t + \frac{\sqrt{\bar{\alpha}_{t-1}}(1 - \alpha_t)}{1 - \bar{\alpha}_t} \frac{1}{\sqrt{\bar{\alpha}_t}} (x_t - \sqrt{1 - \bar{\alpha}_t} \varepsilon_t(x_t, t)) \quad (8)$$

The training object of predict $\mu_{\theta}(x_t, t)$ approximate $\bar{\mu}(x_t, x_0)$ can then replace by predict ε_t given x_t and t . Finally, after disregarding certain coefficient terms, we obtain the loss function in the form of [Equation 3](#), derived from our initial objective function presented in [Equation 7](#).

B More Details for Video Recognition Models

In this work, we used three video recognition models to build our detection and source tracing models. They are Inflated 3D ConvNet [8], Video Masked Autoencoders [54], and X-CLIP [36].

I3D is a convolution-based neural network. Specifically, I3D incorporates a convolution kernel to learn from the temporal dimension. This is described as an advanced version of naive 3D convolution neural networks [29]. This enhancement is achieved by adding batch normalization after each convolution layer. It also extends a pre-trained 2D network to 3D for parameter initialization, addressing the challenges of high parameter count and training inefficiency. X-CLIP directly utilizes the pre-trained CLIP [45] model for video recognition tasks, leveraging its cross-frame attention mechanism to share information across frames. This mechanism enables X-CLIP to capture temporal features effectively. Besides, MAE extends Image AutoEncoders [22] to the video domain. It employs temporal downsampling, cube embedding, and tube masking techniques to devise a novel masked approach. When applied to self-supervised learning by masking multiple frames’ patches, this approach prevents the model from merely learning simple temporal correlations. Instead, it helps the learning of spatial-temporal reasoning about objects.

C More Details for Fake Videos Detection

In Figure 9, we provide several video samples with Grad-CAM. By comparing the I3D-based detection model with the MAE-based detection model. We found that MAE-based detection models are more agile than I3D-based. It can detect inconsistent features in spatial and temporal domains. Therefore achieving a higher detection accuracy.

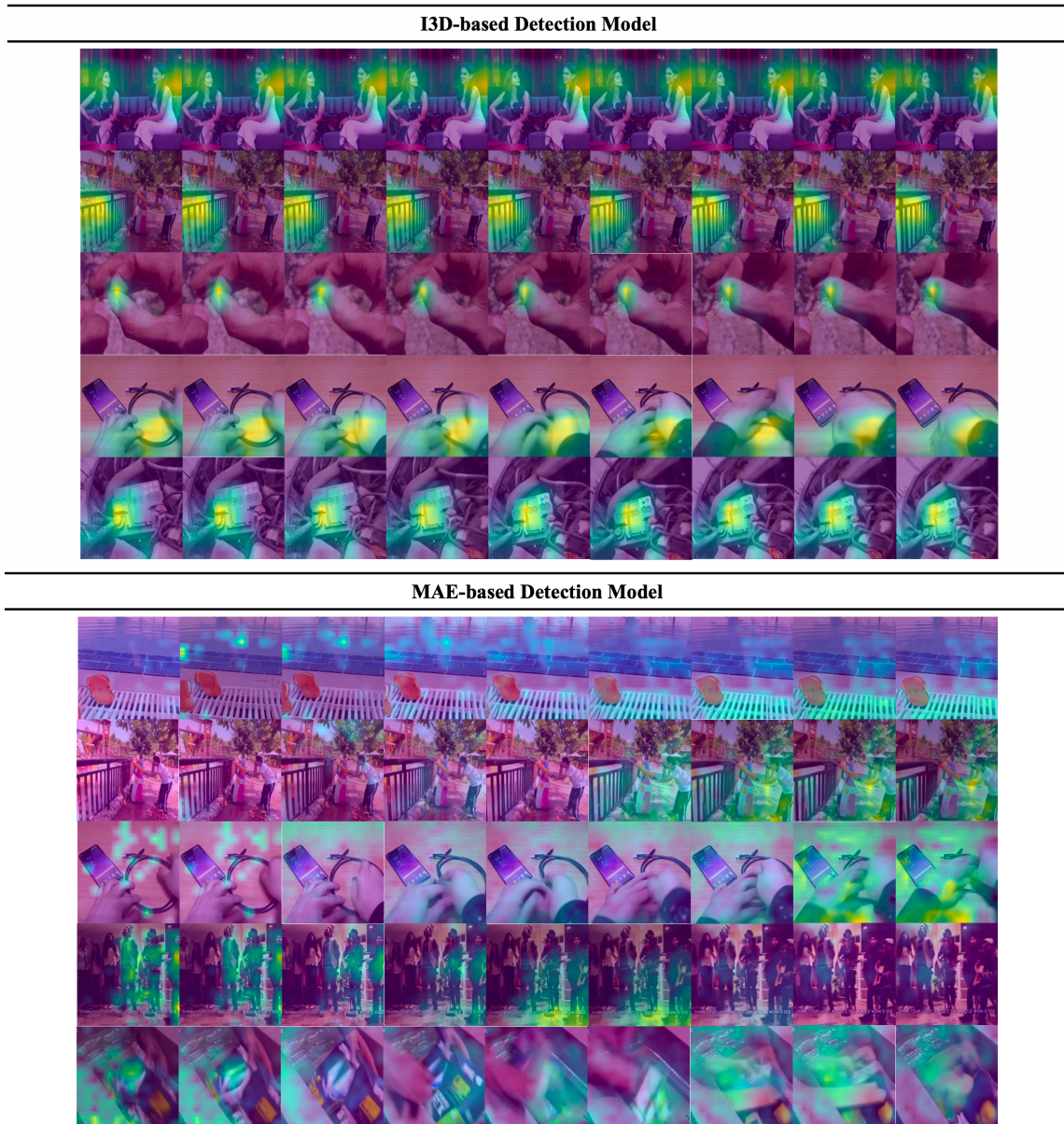
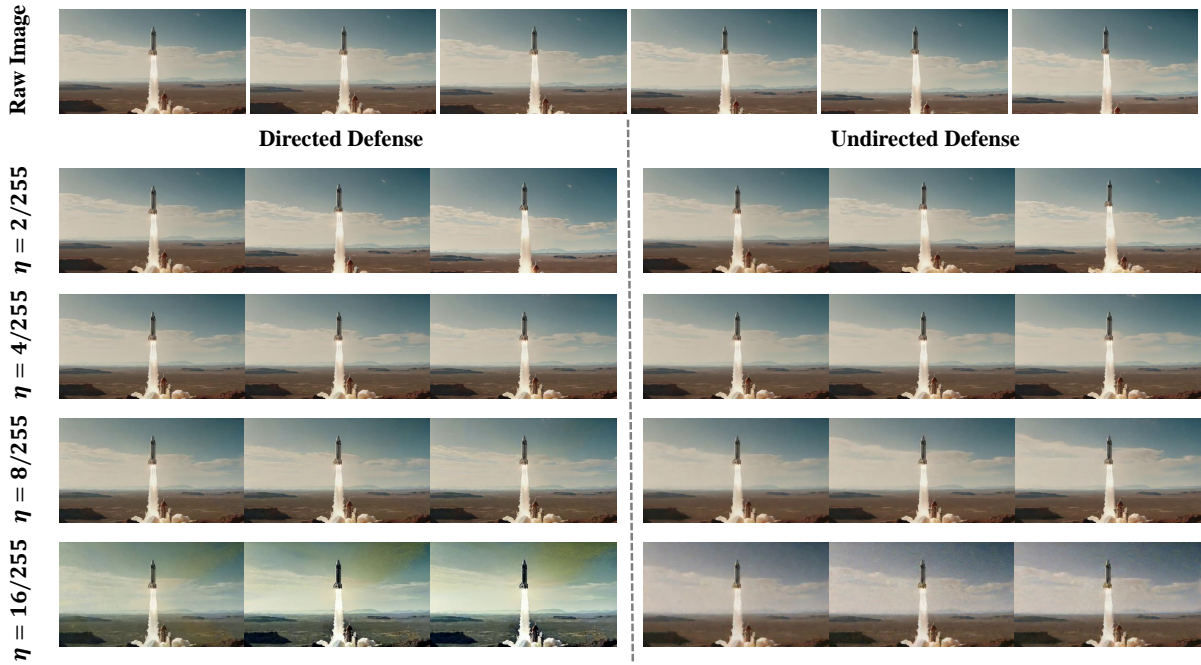
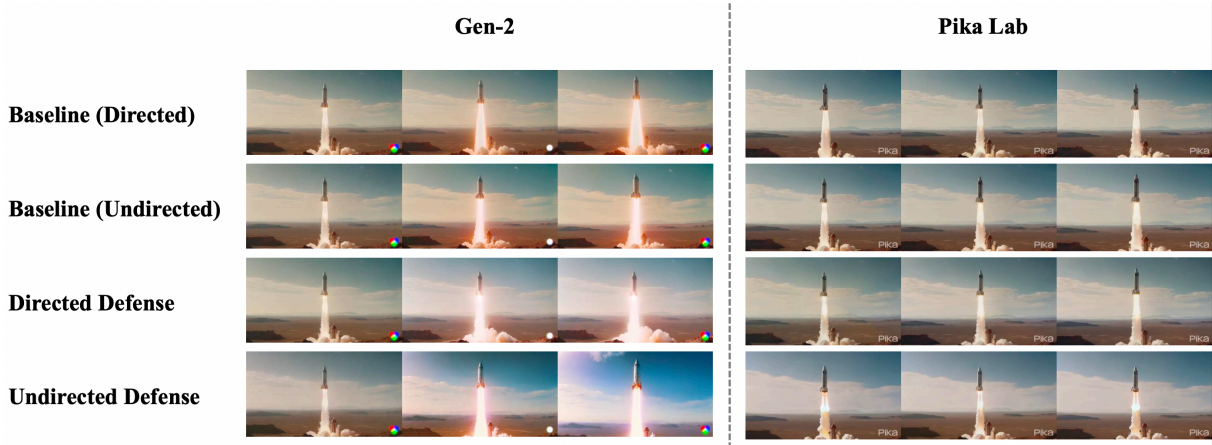


Figure 9: A complete video featuring heatmaps using Grad-CAM on both I3D-based and MAE-based detection models. MAE-based detection model can detect more abnormal points in one video while I3D-based detection model can only detect one place.

D More Details for Misuse Prevention



(a) Demonstrate the defensive efficacy of *directed defense* and *undirected defense* under various η settings.



(b) Comparison between our *directed defense* and *undirected defense* with baseline methods.

Figure 10: Present two defense strategies across various parameters and against different generation models.

We show the supplementary image in Figure 10. Figure 10a showcase *adversarial examples* generated from *directed defense* and *undirected defense*. In Figure 10b, it is evident that for Gen-2, the two baseline methods fail to disrupt the generation process significantly. Notably, the rocket in the video continues to ascend seamlessly into the sky, and the smoke trailing the rocket behaves logically. Our *directed defense* method can effectively immobilize the rocket in mid-air, while the *undirected defense* method. However, it does not significantly interfere with the rocket's movement and can compromise the overall coherence of the video. Conducting tests on the Pika Lab platform revealed that the vanilla videos generated by the model already depict the rocket as stationary. After applying the two baseline methods, the video has no discernible change compared to the original. However, our *directed defense* method succeeds in freezing the motion of the smoke emitted by the rocket, thereby further undermining the video's logical integrity.